AGU PUBLICATIONS

JGR

Journal of Geophysical Research: Atmospheres

RESEARCH ARTICLE
10.1002/2017JD026933

Key Points:
- Relative to background upper tropospheric air, an aerosol enhancement zone (AEZ) exists at the bottom edge of tropical storm anvils
- Storms affected by the SAL have more large particles, likely mineral dust, in the AEZ and these contribute to the background concentration
- Convective lofting of dust by convective systems is predicted to enhance ice nucleating particle concentrations in the upper troposphere

Supporting Information:
- Supporting Information S1

Correspondence to:
C. H. Twohy,
twohy@nwra.com

Citation:
Twohy, C. H., B. E. Anderson, R. A. Ferrare, K. E. Sauter, T. S. L'Ecuyer, S. C. van den Heever, A. J. Heymsfield, S. Ismail, and G. S. Diskin (2017), Saharan dust, convective lofting, aerosol enhancement zones, and potential impacts on ice nucleation in the tropical upper troposphere, *J. Geophys. Res. Atmos.*, *122*, 8833–8851, doi:10.1002/2017JD026933.

Received 7 APR 2017
Accepted 1 AUG 2017
Accepted article online 4 AUG 2017
Published online 31 AUG 2017

Saharan dust, convective lofting, aerosol enhancement zones, and potential impacts on ice nucleation in the tropical upper troposphere

C. H. Twohy[1], B. E. Anderson[2], R. A. Ferrare[2], K. E. Sauter[3], T. S. L'Ecuyer[3], S. C. van den Heever[4], A. J. Heymsfield[5], S. Ismail[2], and G. S. Diskin[2]

[1]NorthWest Research Associates, Redmond, Washington, USA, [2]NASA Langley Research Center, Hampton, Virginia, USA, [3]Department of Atmospheric and Oceanic Sciences, University of Wisconsin, Madison, Wisconsin, USA, [4]Department of Atmospheric Science, Colorado State University, Fort Collins, Colorado, USA, [5]Microscale and Mesoscale Meteorology Laboratory, National Center for Atmospheric Research, Boulder, Colorado, USA

Abstract Dry aerosol size distributions and scattering coefficients were measured on 10 flights in 32 clear-air regions adjacent to tropical storm anvils over the eastern Atlantic Ocean. Aerosol properties in these regions were compared with those from background air in the upper troposphere at least 40 km from clouds. Median values for aerosol scattering coefficient and particle number concentration >0.3 μm diameter were higher at the anvil edges than in background air, showing that convective clouds loft particles from the lower troposphere to the upper troposphere. These differences are statistically significant. The aerosol enhancement zones extended ~10–15 km horizontally and ~0.25 km vertically below anvil cloud edges but were not due to hygroscopic growth since particles were measured under dry conditions. Number concentrations of particles >0.3 μm diameter were enhanced more for the cases where Saharan dust layers were identified below the clouds with airborne lidar. Median number concentrations in this size range increased from ~100 l^{-1} in background air to ~400 l^{-1} adjacent to cloud edges with dust below, with larger enhancements for stronger storm systems. Integration with satellite cloud frequency data indicates that this transfer of large particles from low to high altitudes by convection has little impact on dust concentrations within the Saharan Air Layer itself. However, it can lead to substantial enhancement in large dust particles and, therefore, heterogeneous ice nuclei in the upper troposphere over the Atlantic. This may induce a cloud/aerosol feedback effect that could impact cloud properties in the region and downwind.

1. Introduction

Vast quantities of mineral dust particles are liberated from Saharan soils and then transported over the tropical Atlantic Ocean. Saharan dust particles can act as both cloud condensation nuclei [*Koehler et al.*, 2009; *Karydis et al.*, 2011] and heterogeneous ice nucleating particles [*Chen et al.*, 1998; *Sassen*, 2003; *Hoose and Möhler*, 2012; *Cziczo et al.*, 2013]. They have been found in chemically unprocessed state within individual droplets and ice crystals in clouds off the coast of Africa [*Twohy et al.*, 2009b; *Zipser et al.*, 2009; *Twohy*, 2015]. During Saharan dust transport events across the Atlantic, dust was found to enhance the concentration of ice nucleating particles in the lower troposphere [*DeMott et al.*, 2003], glaciate an altocumulus cloud [*Sassen*, 2003], and dominate cirrus crystal residuals [*Sassen*, 2003; *Cziczo et al.*, 2004]. Several studies have investigated how the dry Saharan Air Layer (SAL) and the dust particles within it influence properties of cloud systems [*Mahowald and Kiehl*, 2003; *Dunion and Velden*, 2004; *Levin et al.*, 2005; *Evan et al.*, 2006; *Jenkins et al.*, 2008; *Herbener et al.*, 2014; *Storer et al.*, 2014; *Herbener et al.*, 2016]. These aerosol indirect effects can have complex manifestations, particularly in clouds where the ice phase is involved [*Khain et al.*, 2005; *van den Heever et al.*, 2006; *Creamean et al.*, 2013; *Fan et al.*, 2013]. Here we focus on how the dust distribution itself is spatially modified by interactions with deep convection and hypothesize that this might induce changes in ice clouds downstream due to redistribution of ice nucleating particles to higher levels in the atmosphere.

Based on CALIOP lidar satellite imagery, *Yu et al.* [2015] estimated that annually, only about 24% of the dust mass leaving the coast of North Africa survives to reach longitude 75°W over the Caribbean Sea. Presumably, the other 76% is deposited in the ocean by wet and dry deposition processes, where it may be important in providing iron and other nutrients to the marine biota [*Jickells et al.*, 2005]. The bulk of the remaining dust stays in the lower free troposphere in the 2–6 km altitude region [*Yu et al.*, 2015]. However, there are some

changes to its vertical structure, particularly along the southern boundary where it interacts with convection [*Liu et al*., 2012]. The tropical upper troposphere aerosol is dominated by recently formed, ultrafine particles [*Brock et al*., 1995; *Weigel et al*., 2011]. Thus, even small quantities of mineral dust lofted and deposited there by storms may change the upper tropospheric background aerosol and impact ice nucleation in downstream clouds. The potential importance of this dust lofting process is investigated here using in situ measurements around convective storms over the eastern Atlantic Ocean.

As they develop, convective storms entrain dry environmental air and detrain cloudy air, which mixes with the external environment. This leads to humid regions around cloud edges containing hydrated aerosol particles and evaporated droplets and ice crystals. These regions have been called cloud "halos" [*Radke and Hobbs*, 1991]. In some studies, they have been called "transition zones" or "twilight zones" [*Koren et al*., 2007]. These terms, while evocative, are not very specific. In addition, "halo" may be confused with a specific optical phenomenon caused by light interaction with ice crystals and does not incorporate the three-dimensional nature of these cloud-perimeter features. Satellite measurements show increases in aerosol optical depth near clouds typically extending 5–15 km or more that may cover significant fractions of the global atmosphere [*Koren et al*., 2007]. Various explanations have been proposed including partly cloudy pixels, new particle production, 3-D cloud reflection effects [*Marshak et al*., 2008], and hygroscopic growth of aerosol particles [*Koren et al*., 2007; *Twohy et al*., 2009a]. Airborne lidar measurements also have detected enhancements in aerosol optical depth near clouds [*Su et al*., 2008; *Eck et al*., 2014].

Most of these previous studies, however, have focused on low clouds where background aerosol concentrations are relatively high due to their proximity to surface sources. Little information is available on transition zones of anvil outflow from deep convection into the typically clean upper troposphere. In the tropics, thunderstorm anvils can reach 16 km in height and extend over 100 s of kilometers horizontally. Here we use in situ measurements to study the edges of convective anvils from deep tropical storms, with the goal of assessing their aerosol characteristics. We find that there is a region of enhanced aerosol scattering and particle number concentration near the base of convective anvils, with particularly large enhancements for convective storms influenced by Saharan dust. A new and explicit name, the "aerosol enhancement zone" is defined for these regions. Using these measured aerosol size distributions and prior measurements of dust and ice nucleating particles, we estimate how much Saharan dust is transported to the upper troposphere by these events and its potential impact on ice nucleation downstream. The in situ measurements of dried aerosol particles presented here are free from partly cloudy pixels, 3-D and hygroscopic growth effects that can confound satellite measurements.

2. Materials and Methods

During the 2006 NAMMA (*NASA African Monsoon Multidisciplinary Analyses*) field program [*Zipser et al*., 2009], aerosol particles and clouds were sampled from the NASA DC-8 aircraft. The aircraft was based about 700 km west of the west African coast at the Cape Verde Islands. The experiment was conducted in August and September 2006, when most African aerosol emissions were from Saharan dust sources to the north. In other seasons, biomass-burning particles from the Sahel are more likely to be mixed with dust sources [*Lieke et al*., 2011; *Rodríguez et al*., 2011].

Data presented here are from 10 flights targeting tropical storm systems and the surrounding environment over the eastern Atlantic Ocean, with various levels of development and dust influence. All samples were in clear air from 8 to 12 km height, levels corresponding to storm anvils and removed from the top of the main SAL layer, which is usually below 6 km [*Ben-Ami et al*., 2009; *Yu et al*., 2015]. Often cloud anvils extended above 12 km to levels that the aircraft could not reach, so our data correspond to heights of the low to middle anvil outflow regions and may include particles sedimenting from above. *Avery et al*. [2010] found that the level of maximum convective outflow in the tropics was 10–11 km, the mode altitude of our sampling. Ambient temperatures at this altitude ranged from 225 K to 255 K. Various time-synced NAMMA measurements (see *Data Availability*) were used to detect cloud edges and to select samples to be included for further analysis, as described below.

Two categories of aerosol samples were compared, those representing the far-field "background" environment, well removed horizontally from the anvil clouds, and those defined as the "precloud edge" (PCE) in clear air immediately prior to the aircraft entering significant anvil cloud (Figure 1). We define "significant"

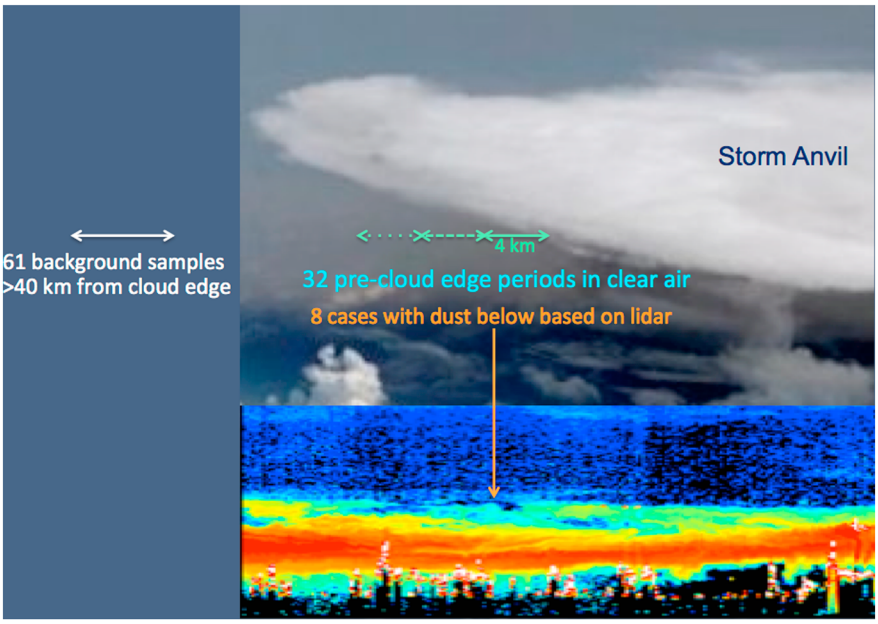

Figure 1. Side view of storm anvil, showing how 32 precloud edge segments were selected for further analysis. Multiple cloud measurements were used to identify the cloud edge, with aerosol data averaged over 20 s (approximately 4 km horizontally) just prior to entering the cloud. Eight of the 32 precloud edges were identified as having dust layers below based on lidar data. Sixty-one background samples were averaged over varying time periods at similar altitudes but at least 40 km horizontally from any cloud. Not to scale. Bottom right shows a dust layer as represented by LASE ASR measurements.

cloud as that having 5 s average condensed water content (CWC) from the counterflow virtual impactor >0.1 g m^{-3}. Reliable aerosol measurements are difficult inside clouds when ice is present, due to the tendency of large hydrometeors to breakup during sampling at aircraft speeds and produce multiple aerosol particles [*Weber et al.*, 1998; *Schwarzenbock and Heintzenberg*, 2000]. A conservative approach using multiple in situ measurements was used to assure that the precloud edge samples had no ice crystals present to compromise aerosol measurements. Thus, each 5 s period had to meet all of the following conditions to qualify as PCE data: ice crystal number concentration from the Cloud Imaging Probe (50–1550 μm diameter) = 0.00 cm^{-3}, CWC $\leq$ 0.001 g m^{-3} and relative humidity with respect to ice (RH_{ice}) from the Diode Laser Hygrometer $\leq$96%. For additional rigor, cloud exit periods were not used to avoid periods where hysteresis may impact CVI measurements [*Heymsfield et al.*, 2007] or where residual artifact particles in sampling lines that could affect aerosol measurements.

Background samples were averaged over available clear-air regions at least 40 km from cloud edges, a distance found to be sufficient to preclude any enhancement in aerosol properties or humidity near the clouds (cf. Figure 3). There were 61 background cases, 32 PCE cases, and a subset of 8 PCE cases with dust below the anvil in the lower troposphere. The latter were selected based on onboard lidar measurements, as described later.

In situ measurements of aerosol microphysical properties and optical parameters were recorded with cabin-mounted instruments sampling downstream of an isokinetic inlet mounted on a window-plate located just ahead of the DC-8 wings [*Chen et al.*, 2011]. The inlet was previously characterized by flying multiple times past an instrumented tower and comparing aerosol scattering and particle size distribution measurements [*McNaughton et al.*, 2007]. That study indicated that 90% to 100% of the particles in the 0.1 to 3 μm diameter range are sampled by instruments downstream of the aircraft inlet, with a 50% sampling efficiency of 5 μm diameter for dust particles. Particle data from precloud edges and background air are presented from three different instruments. The aerosol scattering coefficient at 0.55 μm, $\sigma_{sp,}$ represents the scattering contribution to aerosol optical depth and was determined by a TSI 3563 integrating nephelometer. Data from this instrument were corrected for truncation errors [*Anderson et al.*, 1996] and Rayleigh scattering and represent aerosol scattering over the diameter range from about 0.1 to 5 μm. Ultrafine particle number concentration

>0.003 μm diameter was measured by a TSI 3025A condensation particle counter, while a MetOne optical particle counter (OPC) provided eight channels of size data over the 0.3 to 10 μm diameter range. For both background and PCE samples, relative humidities of ≪10% were typically measured in the aerosol sampling line due to the aircraft cabin temperature being ≥40°C warmer than ambient air. Thus, particles may be considered to be dry for all measurements presented. Also, concentrations are given per ambient volume of air rather than at standard temperature and pressure. More details on the NAMMA aerosol sampling system and instrument suite are provided in *Chen et al*. [2011]. Archived "merge" files containing data from multiple instruments, synced in time, and averaged over 5 s intervals (corresponding to approximately 1 km in horizontal extent) were used for our calculations.

Aerosol scattering ratio (ASR) from the NASA Lidar Atmospheric Sensing Experiment (LASE) lidar on board the DC-8 [*Browell et al*., 1997; *Ismail et al*., 2010] was utilized to identify dust layers below the anvils. LASE provided profiles of water vapor mixing ratio and aerosol scattering ratio at 0.815 μm; the latter is the ratio of aerosol to molecular backscattering corrected for water vapor absorption and attenuation by molecular scattering. LASE transmitted in both nadir and zenith directions simultaneously and so provided profiles both above and below the DC-8. During NAMMA, profiles of aerosol extinction and optical thickness were generated from the LASE data in research mode for some selected cases [*Ismail et al*., 2010]. ASR and aerosol extinction profiles have a vertical resolution of 60 m and a horizontal resolution of 2.1 km. After the precloud edges were identified, simultaneous downward looking LASE scenes were examined to determine if the SAL layer was present below upon approach to the anvil. The SAL was readily visible in LASE ASR images unless midlevel clouds obscured the signal. PCEs where this occurred were not put in the dust category, although it is possible that dust was still present below.

Data from the CALIOP cloud/aerosol lidar aboard the CALIPSO satellite were used to assess dust layers as a function of height in the NAMMA region. Dust aerosols have large particulate depolarization ratios due to the nonsphericity of the particles, allowing them to be distinguished from other aerosol species. Dust particles are identified using an extinction to backscatter ratio at 532 nm of 40 steradians, while polluted dust (a mixture of coarse mode and fine mode clusters) is identified with an extinction to backscatter ratio of 65 steradians [*Omar et al*., 2009; *Winker et al*., 2009]. The CALIPSO cloud aerosol discrimination algorithm was used to determine the certainty of identified cloud or aerosol with high accuracy [*Liu et al*., 2009]. The minimum aerosol optical depth (AOD) threshold of CALIOP in the troposphere is about 0.02–0.04 [*Kacenelenbogen et al*., 2011].

To identify the frequency of storms during the NAMMA time period and region, a cloud product suite based on the Pathfinder Atmospheres Extended (PATMOS-x) algorithm was used. This data set consists of cloud and aerosol properties derived from EUMETSAT's Meteosat Second Generation (MSG) satellite that provides coverage of the NAMMA region from geostationary orbit. The PATMOS-x algorithm has been previously used for AVHRR polar orbiting satellites, while the data used here employ the same algorithm but for the MSG satellites. Cloud data are collected using the Spinning Enhanced Visible and Infrared Imager [*Schmetz et al*., 2002; *Sun et al*., 2015]. MSG supplies significantly enhanced cloud detection and property retrievals from 12 spectral channels [*Schmetz et al*., 2002]. PATMOS-x employs a naïve Bayesian cloud mask algorithm to detect clouds using observed radiances at 1 km resolution and subsamples the results to create an hourly 0.1° × 0.1° resolution grid [*Heidinger et al*., 2012, 2013; *Sun et al*., 2015].

3. Results

3.1. Dry Aerosol Properties: Background Versus Precloud Edge

Figures 2a and 2b show box plots for aerosol scattering coefficient at 0.55 μm and particle concentration >0.003 μm, respectively, for far-field background samples versus the precloud edge samples. For each type of sample, the horizontal black line is the median, the colored box region extends from the lower quartile to the upper quartile of the samples, and the vertical lines include all samples not considered outliers, as defined in the legend. "PCE-All" samples include all 32 precloud edges identified, while "PCE-Dust" samples are the subset of 8 of these identified as having a dust layer below the anvil cloud.

The background samples have a very low scattering coefficient, with the median of 0.2 Mm^{-1}, which is near the noise level of the nephelometer of about 0.11 Mm^{-1} at 0.55 μm for a 5 min averaging period

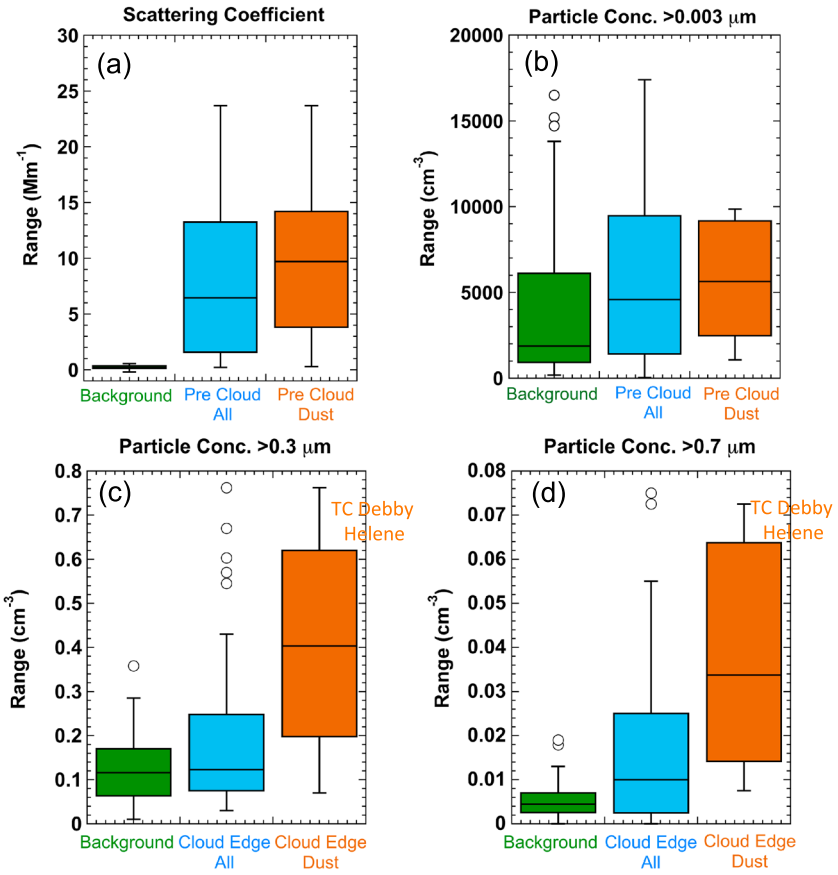

Figure 2. (a) Box plot of aerosol scattering coefficient statistics for background samples (left) versus all precloud edge (PCE) samples (middle) and those for the PCE dust cases (right). Horizontal black line is the median, the colored box region extends from the lower quartile to the upper quartile of the samples, and the vertical lines include all samples not considered outliers. Outliers are defined as points whose values are outside the upper quartile plus 1.5 times the interquartile distance or the lower quartile minus 1.5 times the interquartile distance and are plotted as circles. (b–d) Same as Figure 2a but for particle concentration >0.003 μm, >0.3 μm, and >0.7 μm diameter, respectively.

[*Müller et al.*, 2011]. Scattering at precloud edges is about 30 times higher than background. While this seems a large increase, the median scattering coefficient for the PCEs (~6 Mm^{-1}) is still lower than monthly mean aerosol scattering coefficients in clean marine boundary layer air of 10–30 Mm^{-1} [*Vaishya et al.*, 2011]. The precloud edges of clouds with likely dust influence (PCE-Dust) scatter slightly more light than the PCE population as a whole. Figure 2b shows statistics for particle number concentration >0.003 μm, which is dominated by ultrafine particles. These also increase near cloud edges in the median, but there is a wide range of variability in both the background and PCE samples. Very large values of >5000 cm^{-3} are likely a result of new particles formed in the cold upper troposphere [*Brock et al.*, 1995; *Heintzenberg et al.*, 2011] from gaseous aerosol precursors lofted by convection [*Twohy et al.*, 2002].

Figure 2c shows the concentration of larger particles >0.3 μm measured by the OPC for the different sample types. There is little difference in the median values of the background green box and the blue box representing all PCE samples. However, precloud edges have a much greater range, with a larger upper quartile and several outliers extending to about 7 times the median value. The brown box shows that these outliers are primarily from the dust-influenced cases, where there is about a factor of 4 increase of the median concentration relative to background. For particles >0.7 μm (Figure 2d), there is about a factor of 2 increase in the median values for all cloud PCEs (with high outliers) and about a factor of 8 increase for the PCEs with dust below. Thus, dust-influenced storms have substantially more large particles surrounding their anvil edges than are found in both far-field background and the larger population of anvil edges. In addition, the two dust-influenced cases with the greatest enhancements in large particle concentrations near cloud edges

Table 1. Statistics and Null Hypothesis Test of Difference Between Background (BG) and Precloud Edge (PCE) Aerosol Properties[a]

Parameter	Med[b]	Mean[c] $\overline{x}$	n[d]	df[e]	σ[f]	t_{obs}[g]	t_{crit}[h]	Reject?[i]
BG Scatt	0.2	0.21	61	60	0.17	-	-	-
BG $N > 0.3$ μm	0.12	0.12	61	60	0.071	-	-	-
BG $N > 0.7$ μm	0.0044	0.0052	61	60	0.0039	-	-	-
PCE-All Scatt	6.5	12.6	32	31	18.8	-	-	-
PCE-All $N > 0.3$ μm	0.12	0.21	32	31	0.21	-	-	-
PCE-All $N > 0.7$ μm	0.01	0.019	32	31	0.023	-	-	-
PCE-Dust Scatt	9.7	9.9	8	7	7.8	-	-	-
PCE-Dust $N > 0.3$ μm	0.4	0.41	8	7	0.25	-	-	-
PCE-Dust $N > 0.7$ μm	0.034	0.038	8	7	0.026	-	-	-
Scatt: BG versus PCE-All	-	-	39	89	-	5.17	2.63	Yes
Scatt: BG versus PCE-Dust	-	-	27	65	-	10.2	2.65	Yes
$N > 0.3$ μm: BG versus PCE-All	-	-	39	89	-	3.04	2.63	Yes
$N > 0.3$ μm: BG versus PCE-Dust	-	-	21	65	-	7.34	2.65	Yes
$N > 0.7$ μm: BG versus PCE-All	-	-	18	89	-	4.58	2.63	Yes
$N > 0.7$ μm: BG versus PCE-Dust	-	-	15	65	-	9.50	2.65	Yes

[a]Parameter description: Scatt = dry aerosol scattering coefficient, $N > 0.3$ μm = dry particle number concentration larger than 0.3 μm, $N > 0.7$ μm = dry particle number concentration larger than 0.7 μm.
[b]Median of all samples from the appropriate group: background or precloud edge.
[c]Mean of all samples from the appropriate group: background or precloud edge.
[d]Number of samples in each group.
[e]Degrees of freedom.
[f]σ = sample standard deviation.
[g]Observed t value = $(\overline{x}_{PCE} - \overline{x}_{BG})/s_{\overline{x}_{PCE}-\overline{x}_{BG}}$, where the numerator is the difference in sample means and the denominator is the estimated standard error of the difference.
[h]Critical t value at significance level of 0.01, from statistical tables.
[i]If $t_{obs} > t_{crit}$, null hypothesis may be rejected and differences are considered significant.

were the two strongest storms sampled during NAMMA: Tropical Storm Debby (23 August 2006) and Tropical Depression 8 (12 September 2006) that later became Hurricane Helene. The other storm cases sampled remained as easterly waves, convective troughs that did not develop to named tropical cyclone strength.

Whether the differences between background and PCE aerosol properties are statistically different has been assessed using a two-tailed t test with a significance level of 0.01. T values comparing all aerosol properties shown in Figure 2 are included in Table 1 except for particle concentration >0.003 μm, since its sample values were bimodal, rather than normally distributed. For aerosol scattering coefficient, for particle number concentration >0.3 μm and for particle number concentration >0.7 μm, the t value for the observations, t_{obs}, is greater than the critical t value, t_{crit}. Thus, aerosol properties at the precloud edges are statistically different from the background aerosol properties far from cloud. This applies for the set of all PCEs, as well as for the subset of cases influenced by dust, which exhibit even greater differences between t_{obs} and t_{crit}.

3.2. Extent of Aerosol Enhancement Near the Cloud Boundary

To examine the extent of the aerosol-enhanced region between cloudy and background air, Figures 3a–3d show the changes in aerosol properties as a function of horizontal distance from the cloud edge. To reduce noise, 5 s data were averaged over 20 s intervals, corresponding to approximately 4 km in distance at the aircraft speed. Only the eight cases with dust below, which exhibited the greatest aerosol enhancements, are shown. Aerosol scattering and the concentration of particles >0.3 μm and >0.7 μm all drop off rapidly to background levels ~10–15 km from the cloud edge. However, ultrafine particle concentration (Figure 2b) shows no increase near cloud edges with dust below. This suggests that these anvils are not directly releasing very small particles and that new particle production near clouds may be inhibited in the dust cases. This may be because of the higher aerosol surface area in the outflow region. Under these circumstances, aerosol precursors may condense on existing particles rather than forming new embryos [*Clarke et al.*, 1999] or form them farther away from cloud boundaries.

Of more importance to this investigation, the completely different behavior between aerosol scattering and ultrafine particle concentration (Figures 3a versus 3b) indicates that larger particles, with their high cross-sectional area, are responsible for most of the increase in scattering in dust-influenced anvil outflow

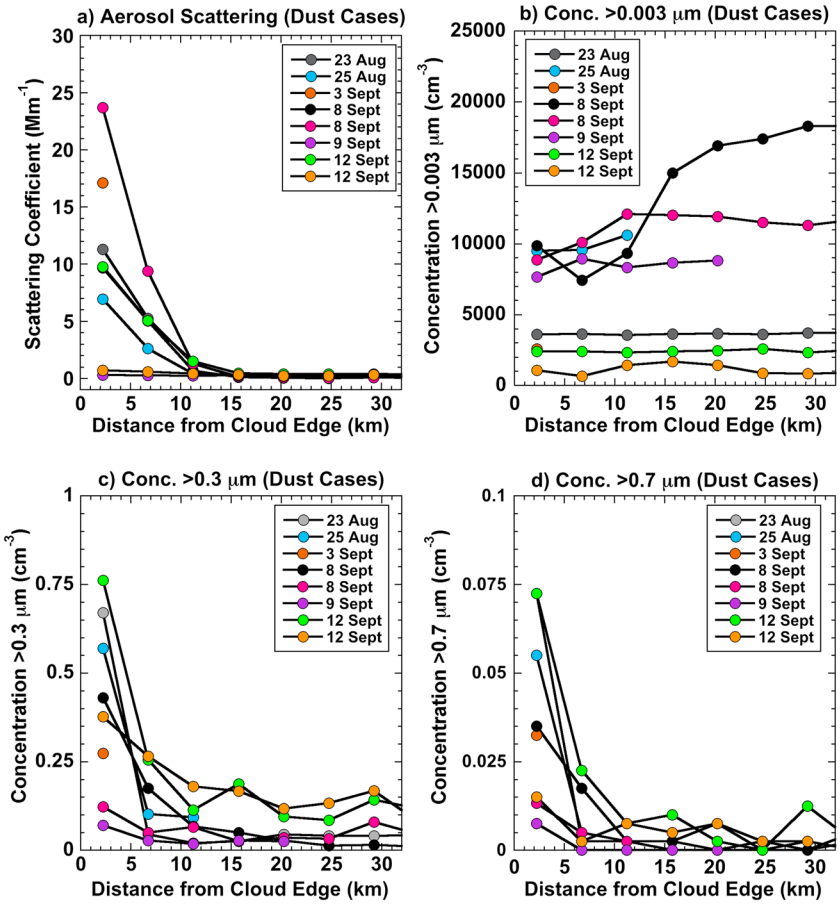

Figure 3. (a) Aerosol scattering coefficient versus distance from the cloud edge for dust cases. (b–d) Same as Figure 3a but for particle number concentration $>$ 0.003 μm, $>$0.3 μm, and $>$0.7 μm diameter, respectively.

regions. The enhancement in concentration of $>$0.3 μm and $>$0.7 μm particles shows a similar, rapid decay pattern that mimics the scattering enhancement out to about ~10–15 km from the cloud edges. While aerosol scattering is often dominated by particles smaller than 0.3 μm, this is not the case if sufficient larger particles are present. For example, *Kleefeld et al.* [2002] showed that aerosol scattering is usually dominated by coarse mode sea salt in the clean marine boundary layer.

The data show that this region of enhanced particles is confined fairly close to the storm, at least for the storms sampled during NAMMA, which were in the developing to mature stages. Interestingly, this distance of 10–15 km is similar to the width of the halos or transition zones observed in the satellite studies described earlier. However, unlike the satellite studies, the aerosol scattering properties presented here were measured inside the aircraft cabin after particles were dried. Given this and the in situ techniques used, the increase near cloud edges measured in this study cannot be attributed to hygroscopic growth, 3-D cloud effects, cloud contamination, or new particle production. For a more precise description of the cloud-to-aerosol transition zone measured in this study, we define the new phrase "aerosol enhancement zone" (AEZ).

A thin AEZ also can be seen in the LASE aerosol scattering ratio, as shown in Figure 4 when the aircraft ascended through the base of the anvil into the main storm on 12 Sept 2006. The anvil cloud itself is imaged as white, where the lidar beam is scattered by ice crystals at ASRs larger than about 30 at high altitudes [*Ismail et al.*, 2010]. The vertical thickness of the AEZ as measured by the lidar is about 0.25 km. Assuming a typical maximum anvil depth of 4 km and radius of 200 km for the NAMMA storm anvils, this zone corresponds to 13 km in horizontal extent when the aircraft transits the sloped anvil base. This value is comparable with the 10–15 km horizontal extent of the AEZ measured in situ (Figure 3). This suggests that the lidar is seeing the same AEZ at the precloud edge as detected with the in situ measurements, which we explore further

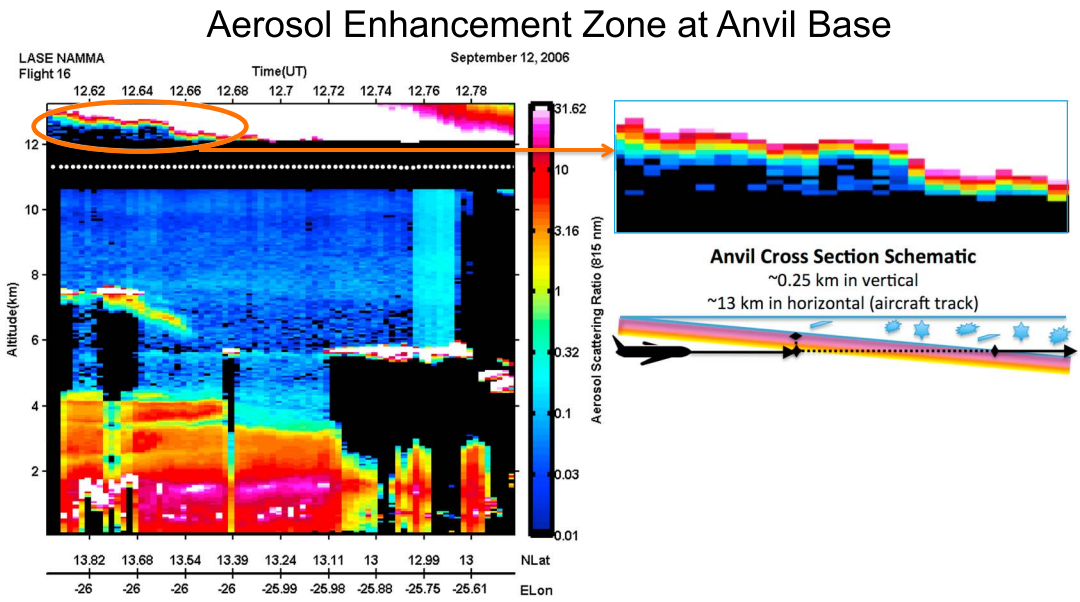

Figure 4. Cross section of aerosol scattering ratio from the LASE lidar during 12 September 2006 flight through the anvil of the storm that became Hurricane Helene. The aircraft track is the dotted white line in the center of the horizontal black zone (the region where the laser beam and telescope field of view are not fully overlapped). Note the thick SAL layer at low altitudes, as well as the ~0.25 km thick zone of intermediate red to yellow scattering ratios at the base of the anvil, which is expanded at the top right. The simplified schematic at middle right (not to scale) shows how the horizontal extent of the enhanced scattering zone as transited by the aircraft is much greater than the vertical extent as measured by the lidar.

below. In addition, ice crystal number concentration in tropical anvils is dominated by irregularly shaped particles with mode maximum dimension 200–300 μm [*Lawson et al.*, 2010]. Falling columnar crystals with a maximum dimension <250–400 μm will sublimate within 200 m at 50% relative humidity and 228 K–240 K [*Hall and Pruppacher*, 1976]. This suggests that the AEZ is primarily a region where ice crystals near the anvil base have sublimated, leaving behind a narrow zone of residual aerosol particles.

The red to yellow values measured by the lidar at the lower border of the anvil have aerosol scattering ratios values ~10 (closest to the cloud edge) to about 0.5 (farther from it). Assuming the molecular backscatter is 0.1 Mm sr^{-1} at 10 km altitude, this would correspond to aerosol backscatter coefficients of about 1 Mm sr^{-1} to 0.05 Mm sr^{-1}. Using an extinction to backscatter ratio (lidar ratio) of 40 for Saharan dust [*Chen et al.*, 2011], this yields extinction coefficients at 0.815 μm of ~40 Mm^{-1} to 2 Mm^{-1} in the AEZ. Since extinction coefficients in NAMMA dust layers were relatively wavelength-independent between 0.45 μm and 0.82 μm [*Ismail et al.*, 2010] and 97% of the light extinction by Saharan dust is due to scattering rather than absorption [*Chen et al.*, 2011], we can compare lidar-derived extinction coefficients of 40 to 2 Mm^{-1} at 0.815 μm to in situ aerosol scattering coefficients at 0.55 μm. Corresponding dry aerosol scattering coefficients measured by the nephelometer for the 12 September AEZ ranged from about 25 to 5 Mm^{-1} (Figure 3a). Thus, despite the instrumental differences and uncertainties, measured extinction properties in the AEZ are remarkably similar for the lidar and nephelometer. Contributing to this agreement between the dried in situ measurements and the ambient lidar measurements are the low median relative humidities in the AEZ, with RH_{ice} values of 63–70% (<50% RH with respect to liquid water), and the relatively low hygroscopicity of Saharan dust [*Koehler et al.*, 2009; *Denjean et al.*, 2015].

The AEZs sampled during NAMMA are geometrically unique from cloud transition zones measured by satellite, which look down at the perimeter of clouds from above [e.g., *Li et al.*, 2014]. Instead, the aircraft-measured NAMMA AEZs occur near the bases of storm anvils, where ice crystals are mixing with dry air and sublimating, releasing their residual aerosol particles back to the atmosphere. These aerosols, being large and having been previously processed by ice particles, potentially become new ice nuclei for clouds formed subsequently. Ice crystal size distributions just within the anvil base were peaked toward smaller crystal sizes and are lower in number concentration than deeper within the cloud, consistent with a region of mixing with

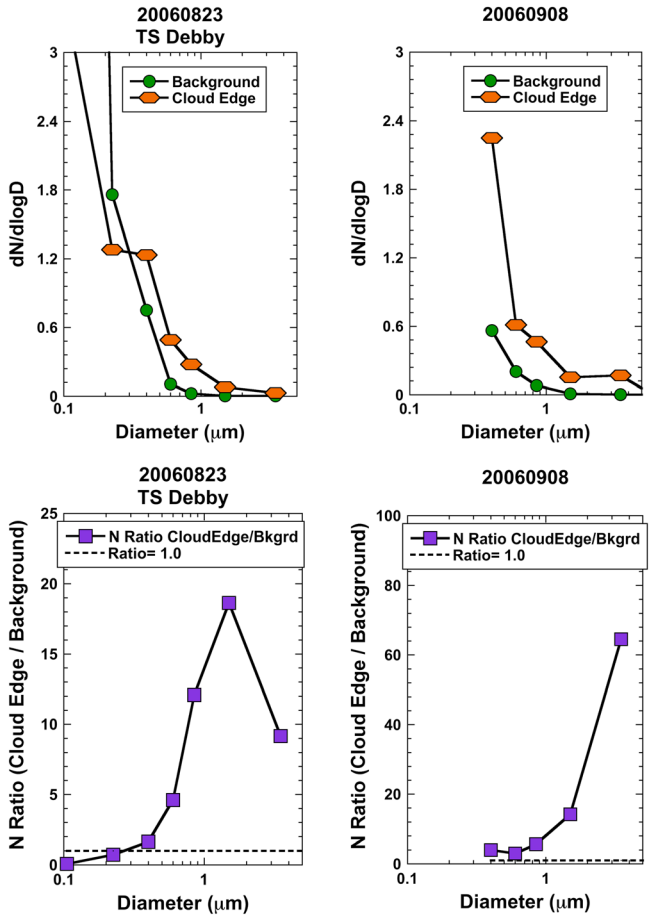

Figure 5. Dry particle size distributions in background air and at anvil precloud edge for two different storm cases. (a) Tropical Storm Debby, including data from for smaller particles from the UHSAS instrument and (b) easterly wave sampled on 8 September 2006. (c and d) The ratio of PCE to background number concentration in each size range.

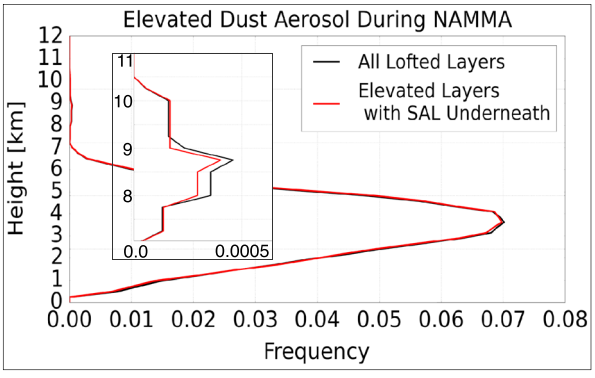

Figure 6. Frequency of occurrence of lofted dust layers detected by the CALIOP lidar for the NAMMA region (5 N–22 N, 10 W–35 W) and time period (August–September 2006). The black line represents all layers that are lofted regardless of the thickness of the layer beneath, while the red line indicates where the lower layer had aerosol optical depths >0.1. Both "dust" and "polluted dust" as described in section 2 are included.

environmental air and sublimation at anvil base. Also, in keeping with a mixing/sublimation zone were the median relative humidities with respect to ice of 70% and 63%, respectively, for all and for dusty AEZs, versus 34% for the far-field background samples.

3.3. Size Distributions

For two different cloud systems with dust influence, aerosol size distributions in the AEZ versus those for background samples on the same flight are shown in Figures 5a and 5b. The first case is for Tropical Storm Debby, while the second is for an easterly wave sampled on 8 September that never developed into a tropical cyclone. For TS Debby, data from an ultra-high-resolution-aerosol-spectrometer (UHSAS) is included to provide data down to smaller sizes. (Since this instrument was experimental and malfunctioned early on, it was not able to be used for the broader statistical analysis given above.) The size distributions verify that substantial enhancement occurs for particles larger than 0.3 μm in the outflow regions of clouds influenced by dust. Figures 5c and 5d show the concentration ratios in the AEZ versus background as a function of size. The ratios are greatest for the largest particles, with enhancements of 10–60 for supermicron particles, consistent with the generally large size of dust aerosol particles [*Chen et al.*, 2011].

3.4. Satellite Measurements of Lofted Dust Layers

CALIOP satellite data were used to determine the frequency of occurrence of dust layers at different altitudes during the NAMMA project time period and region (August–September 2006, 5°N–22°N, 10°W–35°W). Figure 6 shows the frequency of lofted dust layers at each height where "lofted"

means there is a gap between the aerosol layer and either the aerosol layer beneath it or the surface. The large peak at 2–6 km is the SAL itself, while the inset shows a small but significant secondary peak at 8 km to 11 km. Since this is the same altitude as the measured AEZ, this secondary peak likely represents dust particles lofted by convection that remain in the upper troposphere when the anvils dissipate. The black line represents all layers that are lofted regardless of the thickness of the layer beneath, while the red line indicates where the lower layer had aerosol optical depths greater than 0.1, presumably the SAL. Since the red line is almost coincident with the black one, this indicates that most of the detected lofted layers occurred when the SAL was present below. Note that the opposite is not true—i.e., the SAL can exist without upper level layers, since the frequency of 8–11 km layers is much lower than the frequency of the 2–6 km layers. This is because vast areas of the Atlantic can be covered by the SAL without convection being present. In addition, CALIOP may fail to detect layers with AOD below about 0.02–0.04 in the troposphere [*Kacenelenbogen et al*., 2011].

Another interesting feature of Figure 6 is that there are no lofted layers at heights between about 11 and 15 km. While tropical anvil tops could not be reached with the DC-8, NAMMA anvils often extended to these altitudes. Thus, the satellite data support the idea that the AEZ is primarily a phenomenon that occurs near the base of the anvils. We hypothesize the following possible scenario for this. Ice nucleating particles (INP) will preferentially act as heterogeneous INP earlier, at relatively warmer, lower levels in convective updrafts. Other aerosol particle types such as salts and sulfates are most likely to act as homogeneous INP at colder, higher temperatures, as chemical studies of residual ice crystals have shown [*DeMott et al*., 2003; *Twohy and Poellot*, 2005; *Cziczo et al*., 2013]. Ice crystals nucleating on dust therefore would have more time to grow by depositional growth and aggregation and would tend to be larger and more likely to sediment toward the base of the anvil, eventually sublimating. *Lawson et al*. [2010] found that large ice crystals were more prevalent at the lower anvil flight levels in active storms.

4. Dust Particles in the Upper Troposphere and Implications for Ice Nucleation in Downstream Clouds

4.1. Dust Concentrations in the Upper Troposphere

These in situ data are important because they measure dry particle concentration and size directly. Thus, aerosol growth and optical effects that influence satellite studies based on aerosol scattering are avoided. The in situ data demonstrate that increases in aerosol scattering around tropical storm anvils are primarily due to an increase in number concentration of larger, accumulation and coarse mode particles, which dominate particle cross-sectional area and scattering. Storm cases with the SAL layer beneath show the greatest increases in particles >0.3 μm and >0.7 μm. Using median values, number concentrations of particles >0.3 μm in the AEZ are about 400 l^{-1} for clouds influenced by dust. This is consistent with average NAMMA tropical anvil ice concentrations of ~114–630 l^{-1} [*Lawson et al*., 2010] measured using methods that minimize ice crystal shattering [*Jensen et al*., 2009; *Lawson*, 2011]. In addition, anvil residual ice crystal concentrations (>0.1 μm diameter) of 140–660 l^{-1} were measured during NAMMA [*Twohy*, 2015]. This gives further support to the hypothesis that these large particles in the AEZ are primarily residual particles from sublimated ice crystals. Given that the SAL is dominated by dust particles of these sizes [*Chen et al*., 2011], the prevalence of Saharan dust in tropical anvils in the region [*Twohy*, 2015], the greater enhancement of large particles in AEZs with dust below, and the CALIOP data showing dust layers occur at the same altitudes, it is reasonable to assume that the large particles measured in the AEZ are composed primarily of Saharan dust. Midlatitude continental convection was also shown to be an important source of dust to the upper troposphere [*Corr et al*., 2016].

As discussed in section 3.2, the mode size of ice crystals in NAMMA anvils was 200–300 μm [*Lawson et al*., 2010], sizes which will sublimate within about 200 m under conditions in the AEZ [*Hall and Pruppacher*, 1976]. Even much larger crystals with maximum dimension of 800 μm are only expected to survive for about 1.5 km before sublimating [*Hall and Pruppacher*, 1976]. In addition, the settling velocity of a 1 μm dust particle is only ~0.12 mm s^{-1}. Particles ≤ 1 μm that dominate the number concentration in the AEZ will fall less than 100 m in the typical 6 day residence time over the Atlantic (see below). Therefore, dust particles in this size range lofted by deep convection should remain in the upper troposphere for long periods, at least until they are scavenged in subsequent cloud events.

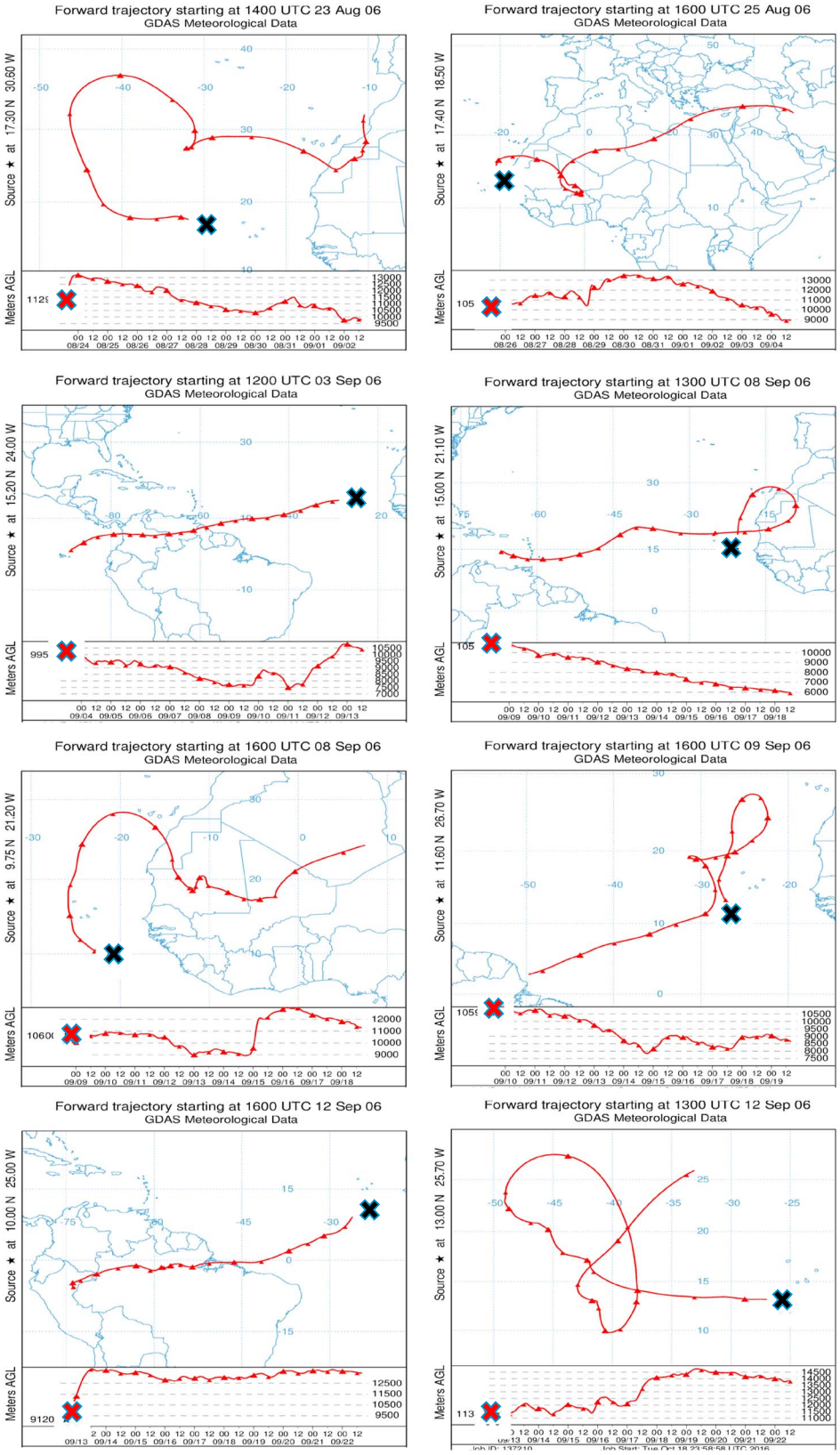

Figure 7. HYSPLIT forward trajectories of air sampled at anvil edges during eight NAMMA storm cases with dust below, originating over the eastern Atlantic at the locations marked with a black X, and originating at the altitude marked with a red X. The Global Data Assimilation System (GDAS) data set was used.

The path of the lower-level SAL is generally westward during hurricane season, with the remnants of the SAL reaching the Caribbean, North America, or the eastern tropical Pacific [*Huang et al*., 2010; *Su and Toon*, 2011]. However, Hybrid Single-Particle Lagrangian Integrated Trajectory (HYSPLIT) forward trajectories for the eight dusty AEZs (Figure 7) indicate that upper tropospheric air originating over the eastern Atlantic can undergo a wide variety of paths in the capricious tropical upper level wind regime. Half the trajectories reach South America or the Caribbean within 10 days, while two end up over Africa. Two are caught in the tropical Azores high and remain primarily over the Atlantic. All except one are predicted to remain above 9 km in the upper troposphere for the entire 10 day period. Five of the eight even ascend up to about 13 km at some point, possibly under the influence of convective motions. On average, outflow air remains over the Atlantic Ocean for about 6 days.

A median concentration of 400 l^{-1} is only 0.4% of the typical concentration of about 90 cm^{-3} particles in the same size range (>0.3 μm) in the SAL itself [*Chen et al*., 2011]. Thus, the number concentration of large particles lofted by convection has negligible influence on the particle population in the SAL itself, consistent with observations [*Twohy*, 2015] and modeling studies [*Herbener et al*., 2016]. This relatively low concentration of dust reaching anvil levels may be due to the ability of Saharan dust particles to act as cloud condensation nuclei as well as ice nucleating particles [*Twohy et al*., 2009b]. Nucleation and coalescence scavenging in droplets and subsequent evaporation and/or wet deposition to the ocean surface therefore likely explain the relatively small percentage of available dust that actually reaches the upper troposphere [*Twohy et al*., 2012; *Herbener et al*., 2016]. While small in terms of the SAL itself, this particle concentration of ~400 l^{-1} in the AEZ at 8–12 km is, however, significantly higher than the background concentration of 100 l^{-1} in the same size range in the upper troposphere. This may have important implications for ice nucleation in the upper troposphere, as discussed below.

4.2. Estimate of Ice Nucleating Particles From Cloud Outflow

The potential concentration of heterogeneous INP in anvil AEZs was estimated first from the median concentration of particles >0.3 μm in the dust-influenced AEZs and an INP parameterization based on immersion freezing measurements of mineral dust particles, including Saharan dust [*DeMott et al*., 2015]. That parameterization uses the number concentration of particles >0.5 μm. Within the SAL itself, concentrations in this size range are about 75% of the number concentration > 0.3 μm [*Chen et al*., 2011], a difference that is taken into account in our calculations. Also, an INP calibration factor of 3 was used, as recommended in *DeMott et al*. [2015]. At the coldest temperatures measured in the *DeMott et al*. [2015] work of 238 K, these assumptions yield about 80 l^{-1} potential immersion INP in the AEZ. (Note that concentrations quoted here are given at typical ambient sampling conditions of 238 K and 260 mb for comparison with ice crystal concentrations, while the DeMott et al. parameterization is formulated in units of standard temperature and pressure (STP). Relative to our conditions, STP concentrations are higher by a factor of 3.3.)

If we assume that the background particle concentration of ~100 l^{-1} in the same size range is also primarily Saharan dust, then immersion INP in the background air would be about 20 l^{-1} at 238 K. Using a more general INP parameterization based on a broad distribution of particle types [*DeMott et al*., 2010], the background INP concentration would only be about 1 l^{-1}. Thus, the dust-influenced AEZ should be enhanced in immersion freezing INP at 238 K relative to the background upper troposphere by a factor ranging from about 4 to 80.

Immersion freezing could be important in subsiding air masses that are later incorporated into midlevel cloud systems, but of more relevance to cirrus formation in the upper troposphere downstream of the AEZs would be nucleation of ice by water vapor deposition. Desert dust can be efficient deposition INP [*Möhler et al*., 2006], particularly at high humidities possible in cloud outflow regions. To convert particle concentrations in the AEZ to potential ice crystal concentrations formed via deposition nucleation, laboratory data from the Aerosol Interaction and Dynamics in the Atmosphere chamber were used [*Ullrich et al*., 2017]. That work utilizes the ice nucleation active surface-site density (INAS) concept, which includes effects of particle surface area as well as environmental conditions. INAS density values between 7.6×10^9 and 3.2×10^{11} m^{-2} were obtained for deposition on Saharan dust (R. Ullrich, personal communication, 2017) under conditions from 220 K < T < 243 K and 1.12 < S_i < 1.42. This encompasses the median AEZ sampling temperature of 234 K and the coldest AEZ sampling temperature of 225 K, as well as slightly colder temperatures possible downstream due to trajectory ascent (Figure 7). Regarding plausible S_i values, *Krämer et al*. [2009] used a

rigorously controlled database measured within cirrus clouds in the upper troposphere and found that clouds were often supersaturated with respect to ice, with S_is occasionally as high as 1.5 (near the homogeneous freezing threshold). Presumably, the higher supersaturations occur in young, developing cirrus [*Kärcher and Lohmann*, 2002] and are more likely to represent the initial conditions leading to ice formation on ice nucleating particles.

To obtain typical dust aerosol surface area in the AEZ, the NAMMA 8 September 2006 case was used because it had a >0.3 μm particle concentration of ~400 l^{-1}, the same as the median value for all dust-influenced cases in Figure 2c. The total surface area of dry particles >0.3 μm measured closest to the cloud edge for that case was 1.2 μm^2 m^{-3}. Using the statistics of *Twohy* [2015], we conservatively assumed that half of the particle concentration >0.3 μm and thus half of the aerosol surface area was composed of Saharan dust for the INAS calculations. Combining this with the high and low INAS given above, predicted ice crystal concentrations that could form via deposition on AEZ dust particles range from 5 to 192 l^{-1} for the median dust-influenced case (for conditions of 220 K < T < 243 K and 1.12 < S_i < 1.42).

This is very near the range of ice crystal number concentrations in isolated tropical cirrus clouds not associated with deep convection of 37–198 l^{-1} [*Lawson et al*., 2010] at temperatures between 239 K and 215 K. Ice concentrations approximately twice as high as the median values would be possible downstream of tropical cyclones impacted by dust (Figure 2c). In addition, the >0.3 μm aerosol surface area for the median AEZ case is about 12 times the aerosol surface area for the median background case, far removed from the convection. These estimates suggest that dust particles lofted by convection are important contributors to the heterogeneous INP concentration in the upper troposphere and can compete with homogeneous nucleation at cold temperatures. This is consistent with the data of *Cziczo et al*. [2013], who found that most cirrus residual particles were composed of mineral dust and metallic compounds.

Most laboratory studies indicate that internal mixtures or "coatings" of mineral dust with nondust compounds can increase the saturation ratio required for deposition nucleation of ice, e.g., *Cziczo et al*. [2009]. These studies are summarized in *Hoose and Möhler* [2012], who state that "Intercomparison between different experiments is difficult because various coating methods have been applied." Nevertheless, their Figure 9 can be used to estimate a median increase in water saturation ratio of 0.11 required to nucleate ice on coated versus uncoated dust (usually Arizona test dust). This is equivalent to a required increase in ice saturation ratio of about 0.16 at 234 K. Interestingly, *Cziczo et al*. [2013] found that ~90% of the mineral dust and metallic residuals from a widespread sampling of cirrus ice contained no apparent sulfate or organic coating. As discussed in *Twohy* [2015], 80% of NAMMA cirrus dust residuals also had no detectable coatings, possibly due to their rapid upward transport in deep convection. These results suggest that most of the dust residuals in the AEZ and later, released from evaporating ice crystals in decaying anvils, should have deposition INP efficiencies similar to uncoated desert dust.

The calculations given above indicate that convective storms interacting with the SAL can produce a significant source of ice nucleating particles to the upper troposphere. In decaying cloud systems, all ice crystals in the anvil will eventually sublimate, leaving an aura of nonvolatile, residual dust particles at and downwind of the anvil location. Many of these are expected to be ice nucleating particles that may enhance heterogeneous ice formation when conditions are favorable for cloud formation in the same region or downstream. This process is hypothesized in Figure 8. Lofting of dust by convection could even result in cloud/aerosol/cloud feedbacks—where increases in cloudiness increase upper tropospheric INP concentrations, which then may change subsequent high cloud cover and the atmospheric temperature profile. Figure 8b includes also the concept of convective invigoration of cloud updrafts [e.g., *Koren et al*., 2005] due to SAL-enhanced CCN. However, because background CCN concentrations in the lower troposphere are much greater than background INP concentrations in the upper troposphere, the convective lofting of INP by storms could be significant even if dust concentrations are too low to significantly enhance CCN and storm dynamics.

4.3. Regional Cloud Frequency, Annual Convective Lofting, and Impact on Background Aerosol Concentrations

Landsea et al. [2009] showed that the number of named Atlantic tropical cyclones (those with maximum sustained surface winds over 33 nm h^{-1}) is currently about 12 per year. NOAA Hurricane Research Division

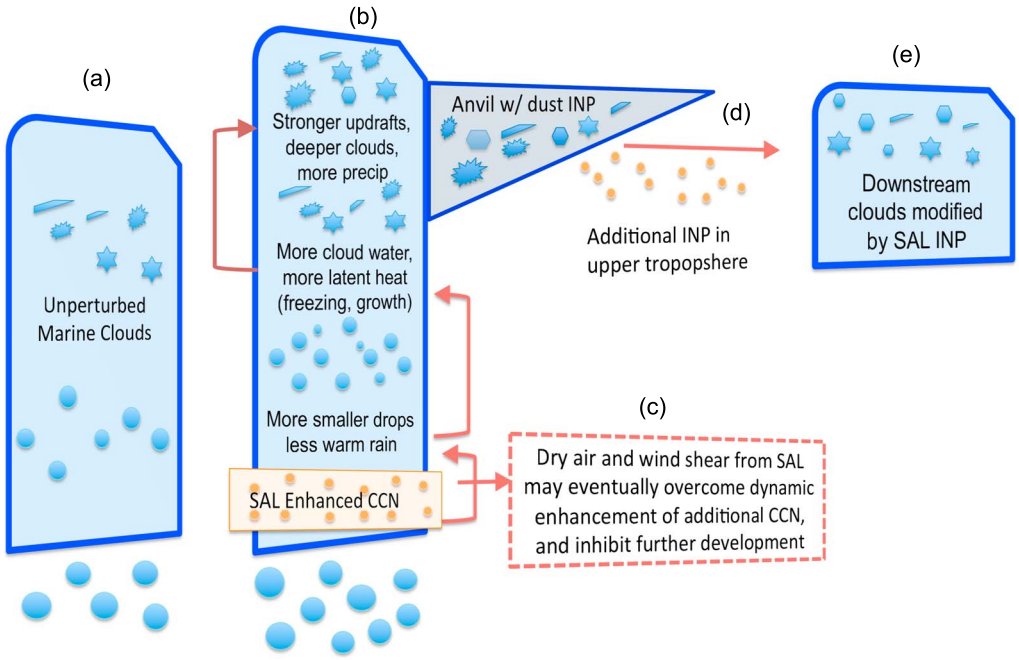

Figure 8. Schematic illustrating important changes that can occur from (a) unperturbed marine clouds when (b) the SAL with its dust aerosol (orange symbols) is present. Additional CCN form smaller droplets (smaller round blue symbols) that can reduce the amount of warm rain (larger round blue symbols). Smaller drops are lofted to colder temperatures where they freeze heterogeneously on dust INP, form ice (blue irregular symbols) and grow. This freezing of water drops and deposition of water vapor produces additional latent heat that can invigorate and deepen the storm. Dry air and wind shear from the SAL inhibit further development and eventually the storm dissipates. (c) Ice particles in the anvil sublimate, leaving enhanced dust INP over a wide region in the (d) upper troposphere. These increased INP have the potential to change the microphysical properties of (e) downstream cirrus clouds.

reports that the annual number of African easterly waves is about 60. NAMMA measurements included two tropical cyclones, Tropical Storm Debby on 23 August 2006 and pre-Hurricane Helene on 12 September 2006. The other easterly waves sampled remained below the tropical cyclone threshold, but most still exhibited enhanced particle concentrations at the PCE (Figure 3).

The aircraft measurements did not, however, include impacts of isolated shallow and deep convection, more organized tropical systems like squall lines, or the convection embedded within the Intertropical Convergence Zone. To investigate the potential importance of other cloud types, the frequency of occurrence of different sizes of deep convective systems observed in the NAMMA region was determined from collocated CALIOP and PATMOS-x data. Using a nearest-neighbor approach, areal footprints with progressively larger radii were created from the data set by averaging an increasing number of pixels around each CALIOP field of view. Convection was then identified in these 13 areal footprints whenever both the mean cloud optical depth exceeded 5 and the mean cloud top temperature was less than 225 K. The size of the convective system associated with each CALIOP field of view was defined as the largest footprint for which both criteria were met. Convection was then identified for all remaining hourly observation times before and after the initial CALIPSO overpass to provide insights into the time evolution of the cloud field around the overpass for a full 24 h period. Cloud frequency of occurrence for each storm size was defined as the number of cloud pixels satisfying these criteria relative to the number of pixels in the NAMMA areal domain (5 N–22 N, 10 W–35 W). To estimate how often convection interacted with the SAL, a third screening was used based on the column dust optical depth beneath the identified convection. *Chen et al*. [2011] found that 90% of NAMMA SAL layers had a median aerosol scattering coefficient greater than 66 Mm^{-1} at 532 nm. Assuming a SAL depth of 4 km (and neglecting extinction due to aerosol absorption which is only a few percent of scattering), this yields an AOD of 0.26. Thus, 0.25 was used as the CALIPSO lidar threshold for the optical depth of the SAL itself in this exercise. Since the lidar becomes fully attenuated in thick clouds, the dust optical depth layer was interpolated to fill in areas where clouds were present.

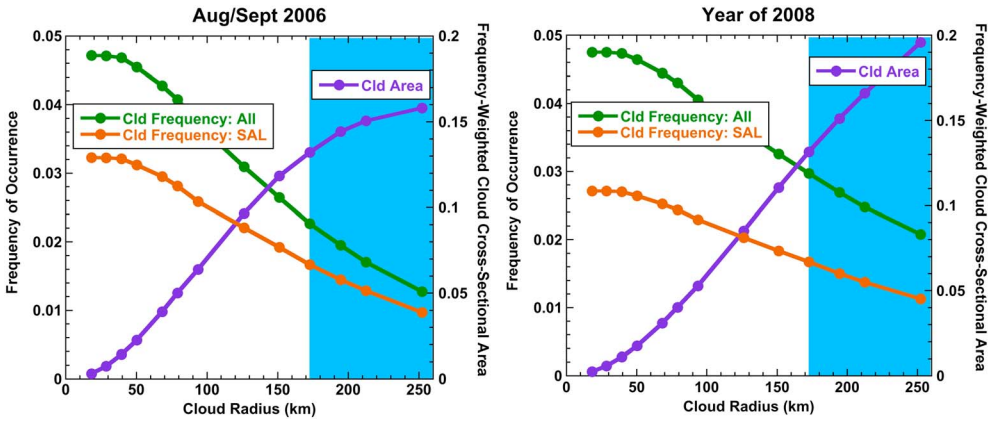

Figure 9. Size and frequency of high clouds for the NAMMA region (5 N–22 N, 10 W–35 W) as determined from PATMOS-x data as described in the text for the August/September 2006 time period (left) and for all of 2008 (right). Frequency for all clouds is shown in green, for clouds with SAL layers beneath in brown, and cloud cross-sectional area weighted by total high cloud area in purple. The blue-shaded regions cover the approximate sizes of dust-influenced anvils of easterly waves and tropical cyclones that were sampled by the aircraft during the NAMMA project.

Cloud frequency statistics were generated for the NAMMA flight period of August/September 2006, as well as for the full year of 2008. (The full year of 2006 could not be used since CALIOP data were not available until the middle of 2006.)

Figure 9 shows the resulting cloud frequency of occurrence (green line) and frequency-weighted cloud cross-sectional area (purple line) as a function of cloud horizontal radius for the NAMMA region. Figure 9a includes August/September 2006 and Figure 9b includes the entire year of 2008. As might be expected, smaller, more isolated systems occur with greater frequency, but larger, more organized storms have greater areal coverage. The blue area includes the approximate anvil sizes of easterly waves and tropical cyclones sampled during NAMMA. These storm sizes account for about half of the high-cloud areal coverage in the eastern Atlantic region during both time periods. Clouds of all sizes frequently have a SAL layer beneath (orange line), on average 71% of the time for clouds during August/September 2006 and 56% of the time for 2008.

These satellite-generated statistics for storms in the vicinity of the SAL were used to generate order-of-magnitude estimates of the number of >0.3 μm particles and dust mass lofted by convection throughout the year, as well as its impact on background concentrations in the upper troposphere. Several assumptions are made from the available data. First, we assume that the concentrations of residual particles that are left in the upper troposphere throughout the dissipated anvil region are similar to concentrations measured in NAMMA AEZs. Utilizing data from these precloud edge regions is a conservative approach, since concentrations of ice and dust nearer the storm center tend to be higher than what we measured near the edges [*Lawson et al.*, 2010; *Twohy*, 2015]. Second, a simplified anvil geometry is used, assuming a round horizontal shape and that a triangular vertical cross sections with an acute peripheral angle of 1.1°. This geometry is based on examination of visible satellite images of the 6 NAMMA dust-influenced storms from the time of sampling, as well as lidar images throughout the project. Third, we assume that half of the 400 l^{-1} particles released by anvils are composed of mineral dust, based on chemical composition of NAMMA anvil ice

Table 2. Estimated Particles Lofted by Convection in NAMMA Region

	# Particles > 0.3 μm Diameter	Dust Mass[a]
Lofted entire year	1.2×10^{23}	0.013 Tg
Diluted concentration[b]	68 l^{-1}	0.78×10^{-6} μg l^{-1}

[a]Assumes 50% of particles are dust and 2.3×10^{-7} μg dust per particle.
[b]Assumes a residence time of 2 days, uniformly distributed throughout the NAMMA upper tropospheric region in a layer 3 km deep.

residuals as measured by *Twohy* [2015]. Finally, as a rough approximation for how background particle concentrations in the upper troposphere may be impacted by these storms, we assumed a residence time of 2 days for anvil-produced particles within the NAMMA region. This is based on the HYSPLIT trajectories' mean residence time of 6 days over the tropical north Atlantic and the NAMMA region covering approximately the eastern third of it.

Table 2 shows the results of this exercise, based on the 2008 cloud frequency data. Throughout the year, about 10^{23} particles >0.3 μm are predicted to be lofted into the NAMMA region by storms, with about half of them expected to be Saharan dust. With an average of ~2.3×10^{-7} μg dust/particle in NAMMA anvils [*Twohy*, 2015], about 0.01 Tg of dust is lofted from the NAMMA region throughout the year. This is a minute amount relative to the 182 Tg of dust leaving the coast of Africa annually [*Yu et al*., 2015] and will have little direct impact on the SAL itself. However, because the upper troposphere is deficient in large particles relative to the lower troposphere [*Delene and Deshler*, 2001; *Clarke and Kapustin*, 2002], this injection of dust particles may impact the background tropospheric concentration of large particles and INP, changing the microphysical and radiative properties of upper level clouds downstream.

The last row of Table 2 shows the result of uniformly distributing particles lofted by convective cloud throughout the NAMMA upper tropospheric region in a layer 3 km deep, assuming a 2 day residence time in the region. Interestingly, the predicted >0.3 μm particle concentration of 68 l^{-1} using this technique, with all its uncertainties, is very similar to the median background concentration of ~100 l^{-1} measured during NAMMA (Figure 2c). These results predict that convective lofting is a significant source of dust aerosol and, consequently, heterogeneous INP in the upper troposphere over the tropical Atlantic. Studies in progress using satellite data to identify and quantify dust layers in the upper troposphere, before and after the passage of convective systems, also corroborate this effect.

These simple calculations assume complete mixing, uniformly averaged over the whole region, while the extent to which particle plumes from anvil remnants may remain coherent is unknown. A low ozone layer lofted by Pacific convection was observed in the upper troposphere 3–5 days from its genesis by *Minschwaner et al*. [2015], and there are certainly indications that Saharan dust influences ice nucleation far from its source. For example, *DeMott et al*. [2003], *Sassen* [2003], and *Creamean et al*. [2013] presented evidence that Saharan dust could act as INP in the midtroposphere over the United States. Additionally, ice residual particles in the upper troposphere over the western Atlantic and eastern Pacific Oceans were dominated by mineral dust and metallic particles, even in marine air masses [*Cziczo et al*., 2013], with similar compositional percentages measured in anvil ice residuals over the eastern Atlantic [*Twohy*, 2015].

5. Discussion

The in situ measurements presented here are consistent with cloud resolving model (CRM) simulations that show small amounts of dust are transported to the upper troposphere by tropical cyclones, with larger amounts removed to the ocean surface [*Herbener et al*., 2016]. They are also consistent with CALIOP satellite investigations that detect upper level dust layers in the vicinity of storms that interact with the SAL (our Figure 6 and *Sauter et al*., 2016]). Number concentrations of particles released to the upper troposphere during NAMMA are smaller than those found around polluted convective storms at midlevels by *Engström et al*. [2008] but may still be significant for ice formation downstream. In the future, sophisticated CRM simulations using Regional Atmospheric Modeling System [*Cotton et al*., 2003; *Saleeby and van den Heever*, 2013] that can track aerosol particles through clouds and regenerate them to the atmosphere will be run for longer time periods to assess potential impacts of convectively lofted INP on downstream cirrus.

There are many uncertainties in how the convective transport of dust will impact climate going forward. Over the past 50 years, dust loadings and transport over the Atlantic have varied in ways that are not fully understood [*Prospero and Mayol-Bracero*, 2013]. Additionally, observations indicate that there has been an uptick in tropical cyclones [*Landsea et al*., 2009] and organized deep convection in recent years that is not predicted by global climate models [*Tan et al*., 2015]. Thus, dust and INP transport to the upper troposphere (and to the ocean surface) may be increasing. If so, net climate impacts are still unclear, since cirrus clouds can either warm or cool the atmosphere depending on their temperature and microphysical characteristics [*Stackhouse and Stephens*, 1991]. Further research efforts in multiple disciplines are needed.

6. Conclusions

A clear-air aerosol enhancement zone exists near the bases of anvils associated with Atlantic tropical storms. This zone has different aerosol characteristics than background air at the same 8–12 km altitude range, with differences significant at the 0.01 probability level. Median dry aerosol scattering coefficient increased by about a factor of 30 adjacent to anvils, and this increase was not due to new particle production or to hygroscopic growth near clouds. Storms with the Saharan Air Layer below transported more large particles to the upper troposphere, with the number concentration of particles >0.3 μm diameter enhanced by about a factor of 4 in the AEZ. This is only ~0.4% relative to dust concentrations in the same size range in the SAL itself but can substantially increase ice nucleating particle concentrations in the upper troposphere when storms dissipate. In addition, simple calculations based on satellite cloud statistics imply that this convective lofting may be responsible for much of the background concentration of large particles (>0.3 μm) in the region. Taken together, the data suggest that lofting of dust and other ice nucleating particles by convective systems may have an extended aerosol indirect effect with impacts on subsequent high cloud formation. Further studies are needed to determine how far downwind of the original convection that dust and INP concentrations may remain elevated and how they impact downstream clouds.

Acknowledgments

We thank Ed Zipser for his foresight and guidance of the NAMMA project. Aaron Bansemer helped with cloud measurements, and Paul DeMott and Eric Jensen provided useful guidance. The NOAA Air Resources Laboratory (ARL) provided the HYSPLIT transport and dispersion model. Data collection was funded by NASA's grant NNX06AC65G (C.T.) and analysis by National Science Foundation grants AGS-1408028 (C.T.), AGS-1409359 (T.L. and K.S.), and AGS-1409686 (S.v.d.H.). Ramesh Kakar and Hal Maring, NASA Headquarters, provided financial support for NASA coauthors. In situ aerosol and cloud data are available in NAMMA LARGE merge files, described and available through archive links here: https://ghrc.nsstc.nasa.gov/opendap/doc/namma/namlarge/namlarge_dataset.html. Images of LASE water vapor mixing ratio, aerosol scattering profiles, and clouds are available at https://science.larc.nasa.gov/lidar/namma/namma.html and are also archived at https://ghrc.nsstc.nasa.gov/uso/ds_docs/namma/namlase/namlase_dataset.html. Cloud frequency data in Figure 9 and used for the calculations in section 11 are available as supporting information.

References

Anderson, T. L., et al. (1996), Performance characteristics of a high-sensitivity, three-wavelength, total scatter/backscatter nephelometer, *J. Atmos. Oceanic Technol.*, *13*(5), 967–986, doi:10.1175/1520-0426(1996)013<0967:PCOAHS>2.0.CO;2.

Avery, M., et al. (2010), Convective distribution of tropospheric ozone and tracers in the Central American ITCZ region: Evidence from observations during TC4, *J. Geophys. Res.*, *115*, D00J21, doi:10.1029/2009JD013450.

Ben-Ami, Y., I. Koren, and O. Altaratz (2009), Patterns of North African dust transport over the Atlantic: Winter vs. summer, based on CALIPSO first year data, *Atmos. Chem. Phys.*, *9*(20), 7867–7875, doi:10.5194/acp-9-7867-2009.

Brock, C. A., P. Hamill, J. C. Wilson, H. H. Jonsson, and K. R. Chan (1995), Particle formation in the upper tropical troposphere: A source of nuclei for the stratospheric aerosol, *Science*, *270*(5242), 1650.

Browell, E. V., et al. (1997), LASE Validation Experiment, in *Advances in Atmospheric Remote Sensing with Lidar: Selected Papers of the 18th International Laser Radar Conference (ILRC)*, edited A. Ansman et al., pp. 289–195, Berlin.

Chen, G., et al. (2011), Observations of Saharan dust microphysical and optical properties from the eastern Atlantic during NAMMA airborne field campaign, *Atmos. Chem. Phys.*, *11*(2), 723–740, doi:10.5194/acp-11-723-2011.

Chen, Y., S. M. Kreidenweis, L. M. McInnes, D. C. Rogers, and P. J. DeMott (1998), Single particle analyses of ice nucleating aerosols in the upper troposphere and lower stratosphere, *Geophys. Res. Lett.*, *25*, 1391–1394, doi:10.1029/97GL03261.

Clarke, A. D., F. Eisele, V. N. Kapustin, K. Moore, D. Tanner, L. Mauldin, M. Litchy, B. Lienert, M. A. Carroll, and G. Albercook (1999), Nucleation in the equatorial free troposphere: Favorable environments during PEM-tropics, *J. Geophys. Res.*, *104*, 5735–5744, doi:10.1029/98JD02303.

Clarke, A. D., and V. N. Kapustin (2002), A pacific aerosol survey. Part I: A decade of data on particle production, transport, evolution, and mixing in the troposphere, *J. Atmos. Sci.*, *59*(3), 363–382, doi:10.1175/1520-0469(2002)059<0363:apaspi>2.0.co;2.

Corr, C. A., et al. (2016), Observational evidence for the convective transport of dust over the Central United States, *J. Geophys. Res. Atmos.*, *121*, 1306–1319, doi:10.1002/2015JD023789.

Cotton, W. R., R. Pielke, R. Walko, G. Liston, C. Tremback, and H. Jiang (2003), RAMS 2001: Current status and future directions, *Meteorol. Atmos. Phys.*, *82*(1), 5–29, doi:10.1007/s00703-001-0584-9.

Creamean, J. M., et al. (2013), Dust and biological aerosols from the Sahara and Asia influence precipitation in the western U. S, *Science*, *339*(6127), 1572–1578, doi:10.1126/science.1227279.

Cziczo, D. J., D. M. Murphy, P. K. Hudson, and D. S. Thomson (2004), Single particle measurements of the chemical composition of cirrus ice residue during CRYSTAL-FACE, *J. Geophys. Res.*, *109*, D04201, doi:10.1029/2003JD004032.

Cziczo, D. J., K. D. Froyd, S. J. Gallavardin, O. Moehler, S. Benz, H. Saathoff, and D. M. Murphy (2009), Deactivation of ice nuclei due to atmospherically relevant surface coatings, *Environ. Res. Lett.*, *4*(4), 044013.

Cziczo, D. J., K. D. Froyd, C. Hoose, E. J. Jensen, M. Diao, M. A. Zondlo, J. B. Smith, C. H. Twohy, and D. M. Murphy (2013), Clarifying the dominant sources and mechanisms of cirrus cloud formation, *Science*, *340*(6138), 1320–1324, doi:10.1126/science.1234145.

Delene, D. J., and T. Deshler (2001), Vertical profiles of cloud condensation nuclei above Wyoming, *J. Geophys. Res.*, *106*, 12,579–12,588, doi:10.1029/2000JD900800.

DeMott, P. J., A. J. Prenni, X. Liu, S. M. Kreidenweis, M. D. Petters, C. H. Twohy, M. S. Richardson, T. Eidhammer, and D. C. Rogers (2010), Predicting global atmospheric ice nuclei distributions and their impacts on climate, *Proc. Natl. Acad. Sci. U.S.A.*, *107*(25), 11,217–11,222, doi:10.1073/pnas.0910818107.

DeMott, P. J., et al. (2015), Integrating laboratory and field data to quantify the immersion freezing ice nucleation activity of mineral dust particles, *Atmos. Chem. Phys.*, *15*(1), 393–409, doi:10.5194/acp-15-393-2015.

DeMott, P. J., K. Sassen, M. Poellot, D. Baumgardner, D. Rogers, S. D. Brooks, A. J. Prenni, and S. M. Kreidenweis (2003), African dust aerosols as atmospheric ice nuclei, *Geophys. Res. Lett.*, *30*(14), 1732, doi:10.1029/2003GL017410.

Denjean, C., S. Caquineau, K. Desboeufs, B. Laurent, M. Maille, M. Quiñones Rosado, P. Vallejo, O. L. Mayol-Bracero, and P. Formenti (2015), Long-range transport across the Atlantic in summertime does not enhance the hygroscopicity of African mineral dust, *Geophys. Res. Lett.*, *42*, 7835–7843, doi:10.1002/2015GL065693.

Dunion, J. P., and C. S. Velden (2004), The impact of the Saharan air layer on Atlantic tropical cyclone activity, *Bull. Am. Meteorol. Soc.*, *85*(3), 353–365, doi:10.1175/bams-85-3-353.

Eck, T. F., et al. (2014), Observations of rapid aerosol optical depth enhancements in the vicinity of polluted cumulus clouds, *Atmos. Chem. Phys.*, *14*(21), 11,633–11,656, doi:10.5194/acp-14-11633-2014.

Engström, A., A. M. L. Ekman, R. Krejci, J. Ström, M. de Reus, and C. Wang (2008), Observational and modelling evidence of tropical deep convective clouds as a source of mid-tropospheric accumulation mode aerosols, *Geophys. Res. Lett.*, *35*, L23813, doi:10.1029/2008GL035817.

Evan, A. T., J. Dunion, J. A. Foley, A. K. Heidinger, and C. S. Velden (2006), New evidence for a relationship between Atlantic tropical cyclone activity and African dust outbreaks, *Geophys. Res. Lett.*, *33*, L19813, doi:10.1029/2006GL026408.

Fan, J., L. R. Leung, D. Rosenfeld, Q. Chen, Z. Li, J. Zhang, and H. Yan (2013), Microphysical effects determine macrophysical response for aerosol impacts on deep convective clouds, *Proc. Natl. Acad. Sci. U.S.A.*, *110*(48), E4581–E4590, doi:10.1073/pnas.1316830110.

Hall, W. D., and H. R. Pruppacher (1976), The survival of ice particles falling from cirrus clouds in subsaturated air, *J. Atmos. Sci.*, *33*(10), 1995–2006, doi:10.1175/1520-0469(1976)033<1995:TSOIPF>2.0.CO;2.

Heidinger, A. K., A. T. Evan, M. J. Foster, and A. Walther (2012), A naive Bayesian cloud-detection scheme derived from CALIPSO and applied within PATMOS-x, *J. Appl. Meteorol. Climatol.*, *51*(6), 1129–1144, doi:10.1175/JAMC-D-11-02.1.

Heidinger, A. K., M. J. Foster, A. Walther, and X. Zhao (2013), The pathfinder atmospheres—Extended AVHRR climate dataset, *Bull. Am. Meteorol. Soc.*, *95*(6), 909–922, doi:10.1175/BAMS-D-12-00246.1.

Heintzenberg, J., M. Hermann, A. Weigelt, A. Clarke, V. Kapustin, B. Anderson, K. Thornhill, P. Van Velthoven, A. Zahn, and C. Brenninkmeijer (2011), Near-global aerosol mapping in the upper troposphere and lowermost stratosphere with data from the CARIBIC project, *Tellus B*, *63*(5), 875–890, doi:10.1111/j.1600-0889.2011.00578.x.

Herbener, S. R., S. M. Saleeby, S. C. van den Heever, and C. H. Twohy (2016), Tropical storm redistribution of Saharan dust to the upper troposphere and ocean surface, *Geophys. Res. Lett.*, *43*, 10,463–10,471, doi:10.1002/2016GL070262.

Herbener, S. R., S. C. van den Heever, G. G. Carrió, S. M. Saleeby, and W. R. Cotton (2014), Aerosol indirect effects on idealized tropical cyclone dynamics, *J. Atmos. Sci.*, *71*(6), 2040–2055, doi:10.1175/JAS-D-13-0202.1.

Heymsfield, A. J., A. Bansemer, and C. H. Twohy (2007), Refinements to ice particle mass dimensional and terminal velocity relationships for ice clouds. Part I: Temperature dependence, *J. Atmos. Sci.*, *64*(4), 1047–1067, doi:10.1175/Jas3890.1.

Hoose, C., and O. Möhler (2012), Heterogeneous ice nucleation on atmospheric aerosols: A review of results from laboratory experiments, *Atmos. Chem. Phys.*, *12*(20), 9817–9854, doi:10.5194/acp-12-9817-2012.

Huang, J., C. Zhang, and J. M. Prospero (2010), African dust outbreaks: A satellite perspective of temporal and spatial variability over the tropical Atlantic Ocean, *J. Geophys. Res.*, *115*, D05202, doi:10.1029/2009JD012516.

Ismail, S., et al. (2010), LASE measurements of water vapor, aerosol, and cloud distributions in Saharan air layers and tropical disturbances, *J. Atmos. Sci.*, *67*(4), 1026–1047, doi:10.1175/2009jas3136.1.

Jenkins, G. S., A. S. Pratt, and A. J. Heymsfield (2008), Possible linkages between Saharan dust and tropical cyclone rain band invigoration in the eastern Atlantic during NAMMA-06, *Geophys. Res. Lett.*, *35*, L08815, doi:10.1029/2008GL034072.

Jensen, E. J., et al. (2009), On the importance of small ice crystals in tropical anvil cirrus, *Atmos. Chem. Phys.*, *9*(15), 5519–5537, doi:10.5194/acp-9-5519-2009.

Jickells, T. D., et al. (2005), Global iron connections between desert dust, ocean biogeochemistry, and climate, *Science*, *308*(5718), 67.

Kacenelenbogen, M., M. A. Vaughan, J. Redemann, R. M. Hoff, R. R. Rogers, R. A. Ferrare, P. B. Russell, C. A. Hostetler, J. W. Hair, and B. N. Holben (2011), An accuracy assessment of the CALIOP/CALIPSO version 2/version 3 daytime aerosol extinction product based on a detailed multi-sensor, multi-platform case study, *Atmos. Chem. Phys.*, *11*(8), 3981–4000, doi:10.5194/acp-11-3981-2011.

Kärcher, B., and U. Lohmann (2002), A parameterization of cirrus cloud formation: Homogeneous freezing of supercooled aerosols, *J. Geophys. Res. 107*(D2), 4010, doi:10.1029/2001JD000470.

Karydis, V. A., P. Kumar, D. Barahona, I. N. Sokolik, and A. Nenes (2011), On the effect of dust particles on global cloud condensation nuclei and cloud droplet number, *J. Geophys. Res.*, *116*, D23204, doi:10.1029/2011JD016283.

Khain, A. P., D. Rosenfeld, and A. Pokrovsky (2005), Aerosol impact on the dynamics and microphysics of convective clouds, *Q. J. R. Meteorol. Soc.*, *131*, 2639–2663.

Kleefeld, C., C. D. O'Dowd, S. O'Reilly, S. G. Jennings, P. Aalto, E. Becker, G. Kunz, and G. de Leeuw (2002), Relative contribution of submicron and supermicron particles to aerosol light scattering in the marine boundary layer, *J. Geophys. Res.*, *107*(D19), 8103, doi:10.1029/2000JD000262.

Koehler, K. A., S. M. Kreidenweis, P. J. DeMott, M. D. Petters, A. J. Prenni, and C. M. Carrico (2009), Hygroscopicity and cloud droplet activation of mineral dust aerosol, *Geophys. Res. Lett.*, *36*, L08805, doi:10.1029/2009GL037348.

Koren, I., Y. J. Kaufman, D. Rosenfeld, L. A. Remer, and Y. Rudich (2005), Aerosol invigoration and restructuring of Atlantic convective clouds, *Geophys. Res. Lett.*, *32*, L14828, doi:10.1029/2005GL023187.

Koren, I., L. A. Remer, Y. J. Kaufman, Y. Rudich, and J. V. Martins (2007), On the twilight zone between clouds and aerosols, *Geophys. Res. Lett.*, *34*, L08805, doi:10.1029/2007GL029253.

Krämer, M., et al. (2009), Ice supersaturations and cirrus cloud crystal numbers, *Atmos. Chem. Phys.*, *9*(11), 3505–3522, doi:10.5194/acp-9-3505-2009.

Landsea, C. W., G. A. Vecchi, L. Bengtsson, and T. R. Knutson (2009), Impact of duration thresholds on Atlantic tropical cyclone counts, *J. Clim.*, *23*(10), 2508–2519, doi:10.1175/2009JCLI3034.1.

Lawson, R. P. (2011), Effects of ice particles shattering on the 2D-S probe, *Atmos. Meas. Tech.*, *4*(7), 1361–1381, doi:10.5194/amt-4-1361-2011.

Lawson, R. P., E. J. Jensen, D. L. Mitchell, B. A. Baker, Q. Mo, and B. Pilson (2010), Microphysical and radiative properties of tropical clouds investigated in TC4 and NAMMA, *J. Geophys. Res.*, *115*, DO0J08, doi:10.1029/2009JD013017.

Levin, Z., A. Teller, E. Ganor, and Y. Yin (2005), On the interactions of mineral dust, sea-salt particles, and clouds: A measurement and modeling study from the Mediterranean Israeli Dust Experiment campaign, *J. Geophys. Res.*, *110*, D20202, doi:10.1029/2005JD005810.

Li, R., H. Cai, Y. Fu, Y. Wang, Q. Min, J. Guo, and X. Dong (2014), The optical properties and longwave radiative forcing in the lateral boundary of cirrus cloud, *Geophys. Res. Lett.*, *41*, 3666–3675, doi:10.1002/2014GL059432.

Lieke, K., et al. (2011), Particle chemical properties in the vertical column based on aircraft observations in the vicinity of Cape Verde Islands, *Tellus B*, *63*(4), 497–511, doi:10.1111/j.1600-0889.2011.00553.x.

Liu, D., Y. Wang, Z. Wang, and J. Zhou (2012), The three-dimensional structure of transatlantic African dust transport: A new perspective from CALIPSO LIDAR measurements, *Adv. Meteorol.*, *2012*, 9, doi:10.1155/2012/850704.

Liu, Z., M. Vaughan, D. Winker, C. Kittaka, B. Getzewich, R. Kuehn, A. Omar, K. Powell, C. Trepte, and C. Hostetler (2009), The CALIPSO lidar cloud and aerosol discrimination: Version 2 algorithm and initial assessment of performance, *J. Atmos. Oceanic Technol.*, *26*(7), 1198–1213, doi:10.1175/2009jtecha1229.1.

Mahowald, N. M., and L. M. Kiehl (2003), Mineral aerosol and cloud interactions, *Geophys. Res. Lett.*, *30*(9), 1475, doi:10.1029/2002GL016762.

Marshak, A., G. Wen, J. A. Coakley, L. A. Remer, N. G. Loeb, and R. F. Cahalan (2008), A simple model for the cloud adjacency effect and the apparent bluing of aerosols near clouds, *J. Geophys. Res.*, *113*, D14S17, doi:10.1029/2007JD009196.

McNaughton, C. S., et al. (2007), Results from the DC-8 inlet characterization experiment (DICE): Airborne versus surface sampling of mineral dust and sea salt aerosols, *Aerosol Sci. Technol.*, *41*(2), 136–159, doi:10.1080/02786820601118406.

Minschwaner, K., et al. (2015), Signature of a tropical Pacific cyclone in the composition of the upper troposphere over Socorro, NM, *Geophys. Res. Lett.*, *42*, 9530–9537, doi:10.1002/2015GL065824.

Möhler, O., et al. (2006), Efficiency of the deposition mode ice nucleation on mineral dust particles, *Atmos. Chem. Phys.*, *6*(10), 3007–3021, doi:10.5194/acp-6-3007-2006.

Müller, T., M. Laborde, G. Kassell, and A. Wiedensohler (2011), Design and performance of a three-wavelength LED-based total scatter and backscatter integrating nephelometer, *Atmos. Meas. Tech.*, *4*(6), 1291–1303.

Omar, A. H., et al. (2009), The CALIPSO automated aerosol classification and lidar ratio selection algorithm, *J. Atmos. Oceanic Technol.*, *26*(10), 1994–2014, doi:10.1175/2009JTECHA1231.1.

Prospero, J. M., and O. L. Mayol-Bracero (2013), Understanding the transport and impact of African dust on the Caribbean Basin, *Bull. Am. Meteorol. Soc.*, *94*(9), 1329–1337, doi:10.1175/BAMS-D-12-00142.1.

Radke, L. F., and P. V. Hobbs (1991), Humidity and particle fields around some small cumulus clouds, *J. Atmos. Sci.*, *48*(9), 1190–1193, doi:10.1175/1520-0469(1991)048<1190:HAPFAS>2.0.CO;2.

Rodríguez, S., A. Alastuey, S. Alonso-Pérez, X. Querol, E. Cuevas, J. Abreu-Afonso, M. Viana, N. Pérez, M. Pandolfi, and J. de la Rosa (2011), Transport of desert dust mixed with north African industrial pollutants in the subtropical Saharan Air Layer, *Atmos. Chem. Phys.*, *11*(13), 6663–6685, doi:10.5194/acp-11-6663-2011.

Saleeby, S. M., and S. C. van den Heever (2013), Developments in the CSU-RAMS aerosol model: Emissions, nucleation, regeneration, deposition, and radiation, *J. Appl. Meteorol. Climatol.*, *52*(12), 2601–2622, doi:10.1175/JAMC-D-12-0312.1.

Sassen, K. (2003), Saharan dust storms and indirect aerosol effects on clouds: CRYSTAL-FACE results, *Geophys. Res. Lett.*, *30*(12), 1633, doi:10.1029/2003GL017371.

Sauter, K. E., T. S. L'Ecuyer, and C. H. Twohy (2016), Impact of convection in the tropical Atlantic Ocean on the processing, transport and redistribution of dust aerosols, paper presented at 96th AMS Annual Meeting, New Orleans, 10–14 Jan.

Schmetz, J., P. Pili, S. Tjemkes, D. Just, J. Kerkmann, S. Rota, and A. Ratier (2002), An introduction to Meteosat second generation (MSG), *Bull. Am. Meteorol. Soc.*, *83*(7), 977–992, doi:10.1175/1520-0477(2002)083<0977:AITMSG>2.3.CO;2.

Schwarzenbock, A., and J. Heintzenberg (2000), Cut size minimization and cloud element break up in a ground based CVI, *J. Aerosol Sci.*, *31*(4), 477–489, doi:10.1016/S0021-8502(99)00535-2.

Stackhouse, P. W., and G. L. Stephens (1991), A theoretical and observational study of the radiative properties of cirrus: Results from FIRE 1986, *J. Atmos. Sci.*, *48*(18), 2044–2059, doi:10.1175/1520-0469(1991)048<2044:ATAOSO>2.0.CO;2.

Storer, R. L., S. C. van den Heever, and T. S. L'Ecuyer (2014), Observations of aerosol-induced convective invigoration in the tropical east Atlantic, *J. Geophys. Res. Atmos.*, *119*, 3963–3975, doi:10.1002/2013JD020272.

Su, L., and O. B. Toon (2011), Saharan and Asian dust: Similarities and differences determined by CALIPSO, AERONET, and a coupled climate-aerosol microphysical model, *Atmos. Chem. Phys.*, *11*(7), 3263–3280, doi:10.5194/acp-11-3263-2011.

Su, W., G. L. Schuster, N. G. Loeb, R. R. Rogers, R. A. Ferrare, C. A. Hostetler, J. W. Hair, and M. D. Obland (2008), Aerosol and cloud interaction observed from high spectral resolution lidar data, *J. Geophys. Res.*, *113*, D24202, doi:10.1029/2008JD010588.

Sun, B., M. Free, H. L. Yoo, M. J. Foster, A. Heidinger, and K.-G. Karlsson (2015), Variability and trends in U.S. cloud cover: ISCCP, PATMOS-x, and CLARA-A1 compared to homogeneity-adjusted weather observations, *J. Clim.*, *28*(11), 4373–4389, doi:10.1175/JCLI-D-14-00805.1.

Tan, J., C. Jakob, W. B. Rossow, and G. Tselioudis (2015), Increases in tropical rainfall driven by changes in frequency of organized deep convection, *Nature*, *519*(7544), 451–454, doi:10.1038/nature14339.

Twohy, C. H. (2015), Measurements of Saharan dust in convective clouds over the tropical eastern Atlantic Ocean, *J. Atmos. Sci.*, *72*(1), 75–81, doi:10.1175/JAS-D-14-0133.1.

Twohy, C. H., and M. R. Poellot (2005), Chemical characteristics of ice residual nuclei in anvil cirrus clouds: Evidence for homogeneous and heterogeneous ice formation, *Atmos. Chem. Phys.*, *5*, 2289–2297.

Twohy, C. H., et al. (2002), Deep convection as a source of new particles in the midlatitude upper troposphere, *J. Geophys. Res.*, *107*(D21), 4560, doi:10.1029/2001JD000323.

Twohy, C. H., J. A. Coakley, and W. R. Tahnk (2009a), Effect of changes in relative humidity on aerosol scattering near clouds, *J. Geophys. Res.*, *114*, D05205, doi:10.1029/2008JD010991.

Twohy, C. H., et al. (2009b), Saharan dust particles nucleate droplets in eastern Atlantic clouds, *Geophys. Res. Lett.*, *36*, L01807, doi:10.1029/2008GL035846.

Twohy, C. H., S. M. Saleeby, S. C. Van den Heever, S. Herbener, and P. DeMott (2012), Interactions between Saharan dust and tropical convection, paper presented at 2012 Fall Meeting, AGU, San Francisco, CA, 3–7 Dec, 2012.

Ullrich, R., C. Hoose, O. Möhler, M. Niemand, R. Wagner, K. Höhler, N. Hiranuma, H. Saathoff, and T. Leisner (2017), A new ice nucleation active site parameterization for desert dust and soot, *J. Atmos. Sci.*, *74*(3), 699–717, doi:10.1175/JAS-D-16-0074.1.

Vaishya, A., S. G. Jennings, and C. Dowd (2011), Seasonal variation of the aerosol light scattering coefficient in marine air of the Northeast Atlantic, *Adv. Meteorol.*, *2011*, 6, doi:10.1155/2011/170490.

van den Heever, S. C., G. G. Carrió, W. R. Cotton, P. J. DeMott, and A. J. Prenni (2006), Impacts of nucleating aerosol on Florida storms. Part I: Mesoscale simulations, *J. Atmos. Sci.*, *63*(7), 1752–1775, doi:10.1175/JAS3713.1.

Weber, R. J., A. D. Clarke, M. Litchy, J. Li, G. Kok, R. D. Schillawski, and P. McMurry (1998), Spurious aerosol measurements when sampling from aircraft in the vicinity of clouds, *J. Geophys. Res.*, *103*, 28,337–28,346.

Weigel, R., et al. (2011), In situ observations of new particle formation in the tropical upper troposphere: The role of clouds and the nucleation mechanism, *Atmos. Chem. Phys.*, *11*(18), 9983–10010, doi:10.5194/acp-11-9983-2011.

Winker, D. M., M. A. Vaughan, A. Omar, Y. Hu, K. A. Powell, Z. Liu, W. H. Hunt, and S. A. Young (2009), Overview of the CALIPSO mission and CALIOP data processing algorithms, *J. Atmos. Oceanic Technol.*, *26*(11), 2310–2323, doi:10.1175/2009JTECHA1281.1.

Yu, H., et al. (2015), Quantification of trans-Atlantic dust transport from seven-year (2007–2013) record of CALIPSO lidar measurements, *Remote Sens. Environ.*, *159*, 232–249, doi:10.1016/j.rse.2014.12.010.

Zipser, E. J., et al. (2009), The Saharan air layer and the fate of African easterly waves—NASA's AMMA field study of tropical cyclogenesis, *Bull. Am. Meteorol. Soc.*, *90*(8), 1137–1156, doi:10.1175/2009bams2728.1.